Organic Materials   B. Liu et al.   THIEME OPEN ACCESS   **Original Article**

Effects of the Electron-Deficient Third Components in n-Type Terpolymers on Morphology and Performance of All-Polymer Solar Cells

Bin Liu[a,b,c]

Huiliang Sun*[a] (ORCID)

Chang Woo Koh[d]

Mengyao Su[a]

Bao Tu[a]

Yumin Tang[a]

Qiaogan Liao[a]

Junwei Wang[a]

Wanli Yang[a] (ORCID)

Hong Meng[b] (ORCID)

Han Young Woo*[d] (ORCID)

Xugang Guo*[a] (ORCID)

[a] Department of Materials Science and Engineering and The Shenzhen Key Laboratory for Printed Organic Electronics, Southern University of Science and Technology (SUSTech), No. 1088, Xueyuan Road, Shenzhen, Guangdong 518055, China

[b] School of Advanced Materials, Peking University Shenzhen Graduate School, Peking University, Shenzhen 518055, China

[c] Department of Physics, National University of Singapore, 2 Science Drive 3, Singapore 117542, Singapore

[d] Department of Chemistry, Korea University, Seoul 136-713, South Korea

sunhl@sustech.edu.cn, hywoo@korea.ac.kr, guoxg@sustech.edu.cn

Abstract Compared with p-type terpolymers, less effort has been devoted to n-type analogs. Herein, we synthesized a series of n-type terpolymers via incorporating three electron-deficient third components including thienopyrroledione (TPD), phthalimide, and benzothiadiazole into an imide-functionalized parent n-type copolymer to tune optoelectronic properties without sacrificing the n-type characteristics. Due to effects of the third components with different electron-accepting ability and solubility, the resulting three polymers feature distinct energy levels and crystallinity. In addition, heteroatoms (S, O, and N) attached on the third components trigger intramolecular noncovalent interactions, which can increase molecule planarity and have a significant effect on the packing structures of the polymer films. As a result, the best power conversion efficiency of 8.28% was achieved from all-polymer solar cells (all-PSCs) based on n-type terpolymer containing TPD. This is contributed by promoted electron mobility and face-on polymer packing, showing the pronounced advantages of the TPD used as a third component for thriving efficient n-type terpolymers. The generality is also successfully validated in a benchmark polymer donor/acceptor system by introducing TPD into the benchmark n-type polymer N2200. The results demonstrate the feasibility of introducing
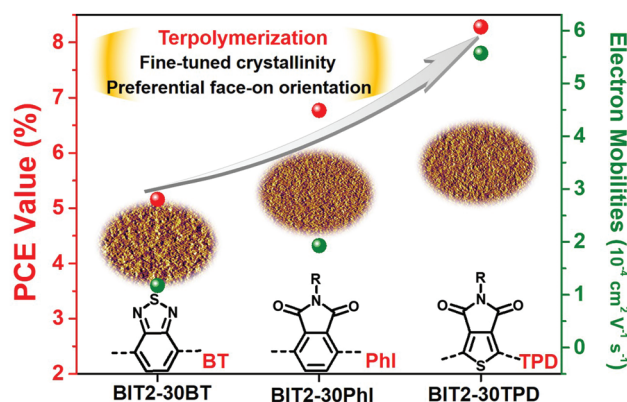
suitable electron-deficient building blocks as the third components for high-performance n-type terpolymers toward efficient all-PSCs.

Introduction

As a promising technology of renewable energy source, organic solar cells (OSCs) with a bulk-heterojunction (BHJ) structure have attracted increasing attention due to their prominent advantages of light weight, low-cost preparation, and huge potential in flexibility, semitransparency and large-area fabrication.[1] In recent years, nonfullerene acceptors have been sprouting up to enhance the ability of capturing solar photon, significantly promoting the development of high-performance OSCs.[2] Among them, all-polymer solar cells (all-PSCs) incorporating a polymeric donor and acceptor as the photoactive layer have emerged as a promising alternative due to their intrinsic merits such as superior morphological stability and mechanical durability.[3] However, their power conversion efficiencies (PCEs) still have lagged behind those of fused-ring electron-acceptor-based OSCs.[4] One of the major challenges to further develop efficient all-PSCs is to achieve a

favorable polymer/polymer blend morphology and packing structure, which can facilitate the charge carrier dissociation and determine PCEs of all-PSCs. To this end, a variety of device methods have been exploited, including cosolvents,[5] solution processing additives,[6] and postdeposition treatment such as solvent vapor annealing.[7] Although the photovoltaic performances of all-PSCs have been successfully progressed to varying degrees, these extra complexities of device fabrication increase time and energy consumption, making the large-area and low-cost industrialization of OSCs a singular challenge.[8]

Recently, the approach of random terpolymerization, which involves the incorporation of a third component into the parent copolymer, has been observed to lead to generation of fine-tuned optoelectronic properties and crystallinity of the resulting terpolymers.[9] In comparison to a large variety of p-type terpolymers with excellent device performance, the development of n-type terpolymers greatly lags behind due to the limited electron-deficient building blocks. Integrating the advantages of available electron-deficient building blocks (introducing the electron-deficient third component into n-type copolymers) to construct random terpolymers with optimized molecular geometry and improved electronic property is a simple and effective approach. For instance, Jenekhe *et al* introduced larger size perylene diimide (PDI) into a naphthalene diimide (NDI)–selenophene copolymer to reduce its strong crystallinity/aggregation and improve compatibility with the polymer donor.[3c] The resulting n-type terpolymer yields a significant enhanced performance (PCE = 6.3% vs. 1.4%). Recently, an electron-deficient dye unit was incorporated into the benchmark n-type copolymer N2200 via random terpolymerization by Chen and coworkers, resulting in not only a reduced crystallinity but also an improved light absorption coefficient and an upshifted LUMO energy level.[9a] Consequently, the n-type terpolymer demonstrated a higher PCE of 8.13% compared to that of N2200 (5.15%). In addition, two similar electron-deficient building blocks containing different side chains were also employed to synthesize terpolymers. For example, an oligoethylene oxide-modified NDI unit was used by Huang *et al.* as the third component in the terpolymerization reaction for morphology optimization.[4d] The resulting NDI terpolymers have achieved an improved PCE with a remarkable fill factor (FF) of up to 75% and excellent stability with 97% of its initial PCE being retained after 300 h of aging at 65 °C compared to the parent polymers. These results clearly suggest that random terpolymerization with the incorporation of the electron-deficient third components is an effective strategy for promoting PCEs in all-PSCs and this strategy enables all-PSCs with improved device stability.

Among various electron-deficient building blocks, fused bithiophene imide (BTI) oligomers have proved to be highly effective ones, e.g., the fused BTI dimer BTI2. The pioneering

work of Osaka and coworkers has manifested that BTI2 is a versatile electron-deficient building block for polymer semiconductors.[10] Our group implements the application of BTI2-based n-type polymers in all-PSCs.[11] These polymers feature much more tunable LUMO levels due to their delocalized topology along polymer backbones compared to classical NDI and PDI-based polymers, which is desirable for reducing energy loss and improving V_{oc} in all-PSCs by minimizing the energy offsets between the polymer donors and acceptors. For example, a copolymer, BTI2-FT (a.k.a. f-BTI2-FT), of BTI2 and 3,4-difluorothiophene shows a PCE of 6.8% with a large V_{oc} of 1.01 V.[12]

Inspired by the success of both terpolymerization-strategy-based two electron-deficient building blocks and BTI2 for developing all-PSCs, here, a series of BTI2-based n-type terpolymers (BTI2-30BT, BTI2-30PhI, and BTI2-30TPD) was designed and synthesized by random polymerization. Therein, three electron-deficient building blocks, benzothiadiazole (BT), phthalimide (PhI) and thienopyrroledione (TPD), with distinct electron-accepting ability and solubility used as the third components were incorporated into the parent polymer BTI2-FT, respectively (Figure 1a). These terpolymers are designed to investigate the effects of the electron-deficient third component on morphological characteristics and photovoltaic properties. They possess sequentially decreasing LUMO energy levels and increased crystallinity from BTI2-30PhI to BTI2-30TPD to BTI2-30BT, leading to distinct energy offset and miscibility when blended with the polymer donor PTB7-Th. Moreover, heteroatoms (S, O, and N) attached to the polymer backbone trigger intramolecular noncovalent interactions, resulting in an increased molecular planarity and having a significant effect on the packing structure. The best PCE was attained from BTI2-30TPD/PTB7-Th combination benefited from promoted electron mobility and face-on polymer packing, which suggested the marked superiority of the electron-
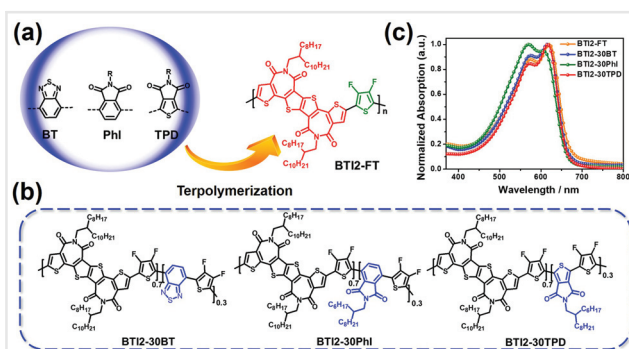
Fig. 1 (a) Terpolymerization via incorporating the electron-deficient third components BT, PhI, and TPD units into the BTI-based polymer BTI2-FT. (b) Chemical structures of BTI2-30X terpolymer acceptors used in this work. (c) UV-vis absorption spectra of neat BTI2-FT and terpolymer films.

deficient third component for developing efficient terpolymer acceptors. This strategy is further validated in PTB7-Th:N2200 blends, where TPD was introduced into the benchmark n-type polymer N2200. The improved PCEs were achieved by TPD-based n-type terpolymers. These results demonstrate the superiority of electron-deficient third components for high-performance n-type terpolymers and pave the way toward high-efficiency all-PSCs.

Results and Discussion

Polymer Synthesis and Properties

Our design for terpolymers is based on previously reported procedures.[12] The copolymers were synthesized by Stille coupling polymerization of the following monomers: f-BTI2-Br, BT-Br, PhI-Br, TPD-Br, and FT (Figure 1b and Scheme S1). The new n-type semiconducting, random BTI-based terpolymers are denoted as BTI2-30X, where X is the co-monomer unit. Based on our previous study, 30% was chosen as the optimal proportion in the BTI terpolymer backbone,[12] i.e., BTI2-30BT (30% BT moiety), BTI2-30TPD (30% TPD moiety), and BTI2-30PhI (30% PhI moiety), respectively (Figure 1b). Meanwhile, the parent copolymer BTI2-FT was synthesized as the reference polymer.[3n] The BTI2-30X samples showed excellent solubility in frequently used organic solvents (e.g., chlorobenzene, dichlorobenzene, and chloroform). The chemical structures of all the terpolymers were confirmed by the ^{1}H NMR data (Figures S10,S11,S12,S13), and their molecular weight (M_n) and dispersity (Đ) were obtained via gel permeation chromatography at 120 °C with 1,2,4-trichlorobenzene as the eluent (Table 1). Thermogravimetric analysis results of all the polymers presented an onset decomposition temperature (T_d) over 380 °C, suggesting their excellent thermal stability in the fabrication and optimization of all-PSCs (Figure S1).

In addition, the normalized UV-vis absorption spectra of the polymer films are shown in Figure 1c and the optical properties are summarized in Table 1. The third compo-

nents possess comparable electron-withdrawing ability with BTI2 in parent polymers, along with intramolecular noncovalent interactions triggered by heteroatoms attached on our terpolymer and the small size of the third components,[9a,7,13] resulting in almost the same intramolecular charge transfer absorption peak at about 400--650 nm.[3n] Despite this, the absorption spectrum for BTI2-30PhI has a slight blue shift compared to those of BTI2-30BT and BTI2-30TPD terpolymers, which is on account of the relatively twisted structure for BTI2-30PhI due to steric hindrance from PhI and adjacent fluorinated thiophene (Figure S3). The optical bandgap (E_g^{opt}) values of these copolymers can be calculated from the absorption onset of films, and are comparably in the range of 1.84–1.88 eV. The HOMO and LUMO levels were obtained by cyclic voltammetry. As displayed in Figures 2b and S2, due to the distinct electron-withdrawing ability of BT, TPD, and PhI units, the sequentially decreasing LUMO energy levels from BTI2-30PhI to BTI2-30TPD to BTI2-30BT can be observed. Their corresponding HOMO/LUMO energy levels were calculated to be −5.27/− 3.39, −5.28/− 3.41, and −5.35/− 3.49 eV, for BTI2-30PhI, BTI2-30TPD, and BTI2-30BT, respectively (Table 1), which showed trends consistent with the density functional theory (DFT) calculation[14] (Figure S3). In addition, the backbone conformation was elucidated by DFT calculation. Benefiting from the reduced steric hindrance between BTI2 and the adjacent thiophene ring along with intermolecular noncovalent interaction induced by the heteroatom attached on polymer backbone, BTI2-30BT and BTI2-30TPD show almost planar geometries. However, there is a 22.8° dihedral angle between PhI and the adjacent 3,4-difluorothiophene, resulting in a relatively twisted molecular backbone and thus a slightly blue-shifted absorption spectrum of BTI2-30PhI.
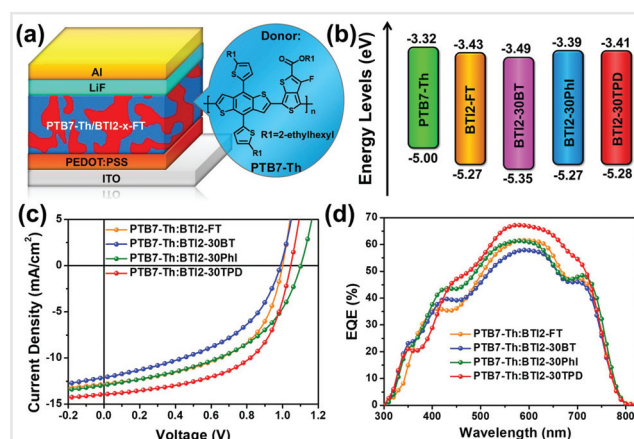

Fig. 2 (a) Device architecture and chemical structure of the donor polymer PTB7-Th. (b) Energy level diagram of PTB7-Th, BTI2-FT, and BTI2-30X terpolymer acceptors. (c) Current density–voltage (J–V) curves under AM 1.5G (100 mW cm^{-2}). (d) EQE spectra of the optimized devices.

Table 1 Basic properties of polymer acceptors BTI2-FT, BTI2-30BT, BTI2-30PhI, and BTI2-30TPD

Polymer acceptor	M_n (kDa)[a]	Đ	λ_{onset} in film (nm)	E_g^{opt} (eV)[b]	HOMO (eV)[c]	LUMO (eV)[c]
BTI2-FT	19.6	2.4	675	1.84	−5.27	−3.43
BTI2-30BT	16.7	2.6	665	1.86	−5.35	−3.49
BTI2-30PhI	12.7	2.3	658	1.88	−5.27	−3.39
BTI2-30TPD	17.6	2.9	663	1.87	−5.28	−3.41

[a]Determined by gel permeation chromatography.
[b]$E_g^{opt} = 1240/\lambda_{onset}$.
[c]HOMO = E_g^{opt} − LUMO.

Photovoltaic Performances

To evaluate the photovoltaic properties of the BTI2-30BT, BTI2-30PhI, and BTI2-30TPD terpolymers, all-PSCs were fabricated using PTB7-Th as the polymer donor with a device structure of ITO/PEDOT:PSS/Active Layers/LiF/Al (Figure 2a). The all-PSCs were prepared after carefully optimizing in terms of D/A ratios, thickness, annealing temperature, and various electron transporting layers (Tables S1–S5). The optimal blend films (D:A = 1:2 wt.%) dissolved in chlorobenzene solvent (total concentration: 16 mg mL^{-1}) were deposited using the spin-coating method without any solvent additives, and the fabricated devices were measured under 100 mW/cm^2 AM 1.5G solar illumination. The typical current density–voltage (J–V) curves of the all-PSCs are shown in Figure 2c and the corresponding photovoltaic parameters are summarized in Table 2. As observed from the J–V curves, the reference PTB7-Th:BTI2-FT solar cell achieved a maximum PCE of 6.84% with a J_{sc} of 12.80 mA/cm^2, a V_{oc} of 1.01 V, and an FF of 52.97%, which are consistent with the previous reports.[12] With the incorporation of the third components in the backbones of polymer acceptors, the V_{oc} of the all-PSCs increased in the order: BTI2-30BT (0.99 V) < BTI2-30TPD (1.05 V) < BTI2-30PhI (1.08 V), due to the gradually decreasing energy offset (ΔE) between the polymer donor PTB7-Th and the terpolymer acceptors (Figure 2b).[15] Notably, profited from the high-lying LUMO levels of the BTI-based n-type polymer, the V_{oc} values of all-PSC devices are basically ≥1.0 V. Interestingly, the PCEs of the terpolymer acceptors displayed a linear component correlation. To be more specific, the corresponding efficiencies increased from 5% to 8% in the sequence BTI2-30BT (5.48%) < BTI2-30PhI (6.80%) < BTI2-30TPD (8.28%), which is in accordance with the observed increase of J_{sc} and FF. For instance, the gradually increasing J_{sc} exhibited the values of 12.11, 12.91, and 13.56 mA cm^{-2} for the terpolymers of BTI2-30BT, BTI2-30PhI, and BTI2-30TPD, respectively. A similar increasing trend for the FF values can also be observed. Obviously, the PCE changes of these terpolymers can be ascribed to the increase of J_{sc} and FF values, which were closely associated with the miscibility and morphology of polymer films (see Figure 4).

To further confirm the accuracy of the J–V results, the external quantum efficiency (EQE) spectra of the BTI2-FT- and BTI2-30X-based PSC devices are plotted and shown in Figure 2d. Similarly, the EQE curves of the all-PSCs displayed both high and broad photoresponses in the spectral range from 300 to 800 nm. The shapes of the curves are consistent with the corresponding absorption spectra, and the integrated J_{sc} values obtained from the EQE spectra are in good agreement (<5% error) with those from the J–V measurements of the optimized devices (Table 2). It is worth noting that the highest photoresponse efficiency (approaching 70%) for the best-performing BTI2-30TPD-based device was achieved throughout the range of 550–650 nm. This result further indicates that the optimal film morphology is effectively conducive to the light harvesting and photocurrent in the all-PSCs.

Crystallinity, Packing Structures, and Morphology of Polymer Films

To probe into the intramolecular stacking and nanostructured order of polymer films, 2D grazing-incidence wide-angle X-ray scattering (GIWAXS) measurement was conducted on the neat and blend thin films of the terpolymers. A 30 − 40 nm thin layer of PEDOT:PSS was spin-coated on the silicon substrate, and the neat or blend polymer films were prepared by spin-coating on the PEDOT:PSS layer. The GIWAXS images and in-plane (IP) and out-of-plane (OOP) line-cut patterns of BTI2-FT and BTI2-30X films are depicted in Figures 3a–d and i–j, and their corresponding packing parameters are included in Table S6. All the neat films showed strong (100) lamellar scattering peaks at ~0.24 Å^{-1} along the IP (q_{xy}) and OPP (q_z) directions, which corresponded to a lamellar d-spacing of ~26.0 Å. As BT, TPD, and PhI were incorporated into the BTI2-FT polymer backbone, the π–π stacking distance in the IP direction for the BTI2-30BT and BTI2-30TPD films remained almost unchanged at ~3.56 Å, while the BTI2-30PhI film showed a

Table 2 Optimized photovoltaic performance parameters of the all-PSCs using BTI2-FT or BTI2-30X as the electron acceptor and PTB7-Th as the electron donor under the Illumination of AM 1.5G, 100 mW cm^{-2}

Active layer[a]	V_{oc} (V)[b]	J_{sc} (mA cm^{-2})[b]	Cal. J_{sc} (mA cm^{-2})[c]	FF (%)[b]	PCE (%)[b]
PTB7-Th:BTI2-FT	1.01 (1.00 ± 0.03)	12.80 (12.54 ± 0.26)	12.39	52.97 (51.53 ± 1.44)	6.84 (6.46 ± 0.38)
PTB7-Th:BTI2-30BT	0.99 (0.97 ± 0.02)	12.11 (11.93 ± 0.18)	11.52	45.80 (43.75 ± 2.05)	5.48 (5.06 ± 0.42)
PTB7-Th:BTI2-30PhI	1.08 (1.06 ± 0.02)	12.91 (12.79 ± 0.12)	12.43	48.75 (47.29 ± 1.46)	6.80 (6.41 ± 0.39)
PTB7-Th:BTI2-30TPD	1.05 (1.05 ± 0.01)	13.56 (13.46 ± 0.10)	13.32	58.25 (57.24 ± 1.01)	8.28 (8.10 ± 0.18)

[a]The device area is 4.5 mm^2.
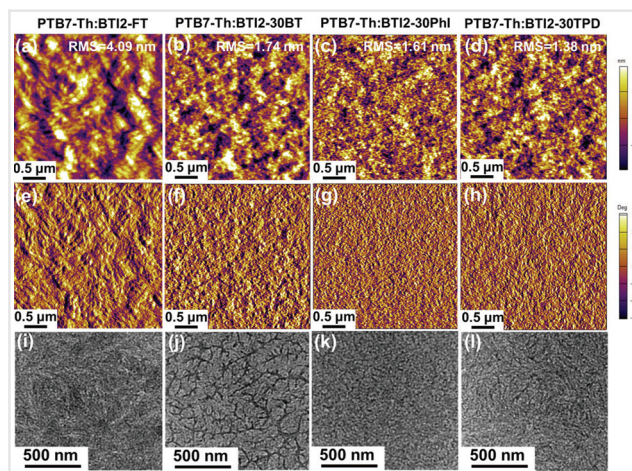[b]Average values with standard deviation were obtained from 20 devices.
[c]J_{sc} integrated from the EQE curve.

218

Organic Materials   B. Liu et al.   THIEME OPEN ACCESS   **Original Article**
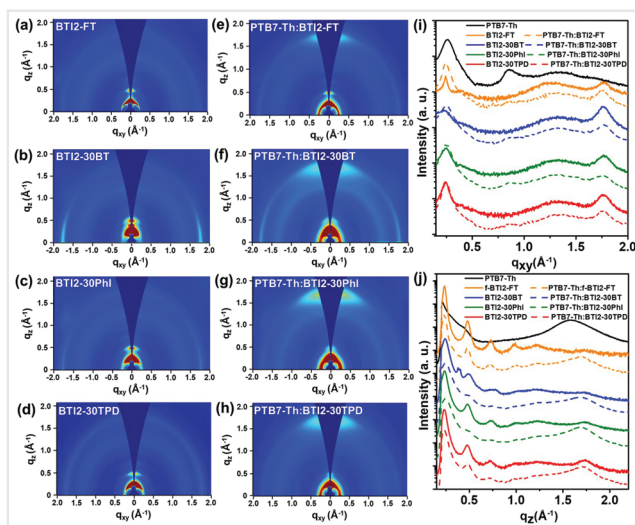
Fig. 3 (a–d) 2D GIWAXS images of the BTI2-FT and BTI2-30X neat films. (e–h) 2D GIWAXS images of the PTB7-Th:BTI2-FT and PTB7-Th:BTI2-30X blend films; (e) in-plane and (f) out-of-plane line cuts of GIWAXS patterns of all neat and blend films.

Fig. 4 AFM height images (a–d), phase images (e–h), and TEM images (i–l) of the PTB7-Th:BTI2-FT and PTB7-Th:BTI2-30X blend films.

slightly larger π–π stacking distance of 3.58 Å due to the twisted polymer backbone, which was in accordance with the UV-vis absorption of these terpolymers. Nevertheless, in general, the irregularity of the terpolymer backbone can still lead to a decrease in the crystallinity of the terpolymer. Besides, the neat BTI2-30BT shows an edge-on dominant orientation, while an increased face-on packing structure was observed for the terpolymers BTI2-PhI and BTI2-30TPD, which is likely related to the noncovalent S⋯O interaction.[3n16b] These were in good agreement with electron mobilities of the neat films measured by space charge limited current method (SCLC; Table S10).[16]

In the PTB7-Th:BTI2-30X blend films, the decreased diffraction peak intensities as a function of introduced BT, TPD, and PhI in blend films suggest a relatively reduced crystallinity in the terpolymer-based blend films, which is closely related to the miscibility and compatibility with PTB7-Th.[3c] In addition, an enhanced face-on orientation was observed in terpolymer-based blends, specifically, a gradually increase in face-on packing structures with more close π–π stacking in OOP (010) orientations was observed from BTI-30BT to BTI-30PhI to BTI-30TPD. This observed trend was similar to that of neat films due to effects of the intramolecular noncovalent interactions and improved miscibility (Table S7). Such a situation has also been observed in other type of PSCs based on fullerene and fused-ring electron acceptors.[16b17] In our case, S⋯O and S⋯F noncovalent interactions in BTI2-30TPD were likely beneficial for promoting a planar π-backbone and interchain ordering with better solution processability, which can contribute to the charge carrier transport in the vertical direction, thereby improving the J_{sc} values for the BTI2-30TPD-based all-PSC devices.

The BHJ surface and bulk morphologies of the PTB7-Th:BTI2-30X blend films as well as the reference PTB7-Th:BTI2-FT polymer blend were investigated by tapping-mode atomic force microscopy (AFM) and transmission electron microscopy (TEM). As displayed in Figure 4a–h, the as-cast PTB7-Th:BTI2-FT thin film exhibited a large-scale phase separation with a root mean square roughness (R_q) of 4.09 nm.[18] As the co-monomer units (BT, PhI, and TPD) were incorporated into the pristine BTI2-FT polymer, a dramatic change in film morphology was observed, and a much smoother surface was obtained. The R_q values decreased from 4.09 nm for the PTB7-Th:BTI2-FT blend to 1.74, 1.61, and 1.38 nm for the BTI2-30BT-, BTI2-30PhI-, and BTI2-30TPD-based blends, respectively, due to the irregular polymer backbone.[3n19] Additionally, the TEM measurements (Figure 4i–l) demonstrated a gradual definite fibril structure stemmed from a bicontinuous interpenetrating network. In particular, the random BTI2-30TPD-based blend film was inclined to form a highly uniform and prominent nanofibrillar morphology, which agreed well with the R_q value and the significantly quenched photoluminescence efficiency (Figure S7). Thus, the favorable bulk morphology in the BTI2-30TPD-based blend led to a more effective exciton dissociation and charge transport, thereby boosting the J_{sc} and FF in the all-PSCs.

Charge Dissociation, Recombination, and Transport Characteristic

To evaluate the charge generation and charge collection processes, photocurrent density ($J_{ph} = J_{light} − J_{dark}$) versus effective voltage ($V_{eff} = V_0 − V_{app}$) curves were plotted for the investigated all-PSCs. Here, V_0 refers to the built-in voltage and V_{app} is the applied voltage. As depicted

219

Organic Materials   B. Liu et al.   THIEME OPEN ACCESS   **Original Article**
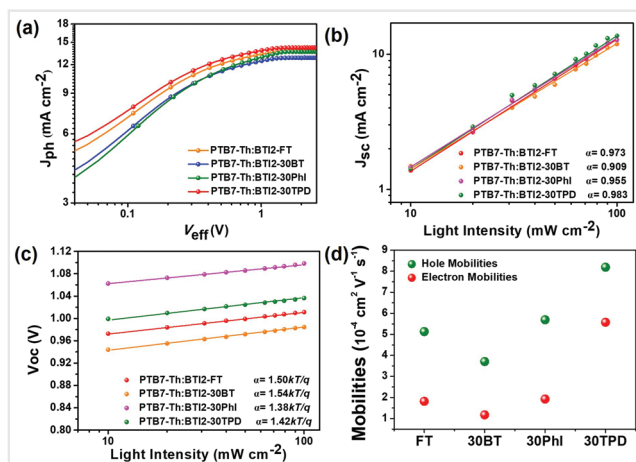
Fig. 5 (a) P_{diss} versus V_{eff} plots, (b) dependence of J_{sc} on different light intensity, (c) light intensity dependence of V_{oc}, and (d) electron and hole SCLC mobilities of all-PSCs based on BTI2-FT or BTI2-30X polymer acceptors.

in Figure 5a, The J_{ph} values saturate at a high V_{eff} of ~1.0 V, giving rise to saturation photocurrent densities (J_{sat}) of about 12.84 mA cm^{-2} in BTI2-30BT, 13.65 mA cm^{-2} in BTI2-30PhI, and 14.21 mA cm^{-2} in BTI2-30TPD (Table S8). At the near-saturation point, the effective voltage (V_{eff}) is large enough to dissociate almost all the photogenerated free excitons, suggesting the excellent carrier extraction capability of all the polymer/polymer blends. Next, the charge collection probability (P_{diss}) was calculated by $J_{\text{ph}}/J_{\text{sat}}$ to investigate the charge carrier collection ability of the PTB7-Th:BTI2-30X blends under short-circuit conditions. The P_{diss} values were determined to be 92.73%, 93.74%, and 95.24% for the BTI2-30BT-, BTI2-30PhI-, and BTI2-30TPD-based devices, respectively, which are in agreement with the corresponding PL quenching efficiencies. The higher P_{diss} value indicated that a more effective exciton dissociation and collection occurred in the PTB7-Th:BTI2-30TPD device in comparison with the other all-PSCs. This result implies that there can form more favorable bulk morphologies in the BTI2-30X-based blends with the incorporation of the BT, PhI, and TPD electron-deficient units in sequence, ultimately resulting in greatly enhanced J_{sc} in BTI2-30TPD-based devices.[3g]

In order to explore charge carrier recombination kinetics, the J_{sc} value as a function of light intensity (P_{light}) was measured using the equation: $J_{\text{sc}} \propto P_{\text{light}}{}^{\alpha}$, thereinto α ~ 1 means negligible bimolecular recombination.[20] The determined α values were 0.973, 0.955, and 0.983 for PTB7-Th:BTI2-FT, PTB7-Th:BTI2-30PhI, and PTB7-Th:BTI2-30TPD, respectively (Figure 5b). These results suggest the relatively suppressed charge recombination in their corresponding devices. In contrast, the α value for the BTI2-30BT-based device was merely 0.909, which corre-

sponded to the poor FF performance. Additionally, the P_{light} dependence of V_{oc} was also applied to study the geminate recombination loss. As seen in Figure 5c, all the BTI2-30X-based devices exhibited a small dependence of V_{oc} on P_{light} with a slope of $1.3 - 1.5\ kT/q$, indicating a reduced geminate recombination loss. These results further suggest that the enhanced J_{sc} values of the PTB7-Th:BTI2-30TPD devices were indeed due to the favorable microstructural compatibility via introducing TPD units to the pristine BTI2-FT polymer.

Furthermore, the bulk vertical hole and electron mobilities in the neat and all-polymer blend films were measured to explore the charge transport characteristics via the SCLC method.[21] The $J^{1/2} - (V_{\text{appl}} - V_{\text{bi}})$ curves and SCLC data are plotted in Figures 5d and S4, S5, S6, and the charge carrier mobilities are included in Tables S9 and S10. For the neat films, the calculated electron mobility (μ_{e}) of the BTI2-FT neat film was 2.40×10^{-4} cm^2 V^{-1} s^{-1}. By contrast, the μ_{e} values for the PhI and TPD unit-incorporated terpolymers were significantly improved. In particular, the electron mobility increased by about threefold in the BTI2-30TPD films ($\mu_{\text{e}} = 7.11 \times 10^{-4}$ cm^2 V^{-1} s^{-1}, which was the highest mobility value among the four polymer acceptors). Similarly for the blend films, hole mobilities (μ_{h}) of 3.71×10^{-4}, 5.69×10^{-4}, and 8.19×10^{-4} cm^2 V^{-1} s^{-1} for BTI2-30BT, BTI2-30PhI, and BTI2-30TPD were obtained, and the corresponding μ_{e} values were 1.18×10^{-4}, 1.93×10^{-4}, and 5.57×10^{-4} cm^2 V^{-1} s^{-1}, respectively. Clearly, the substantial increase of charge carrier mobilities indicated that a more beneficial bulk morphology has been tuned in the BTI2-30TPD blend, leading to more efficient charge transporting than the reference BTI2-FT blends. Moreover, a more balanced charge mobility ($\mu_{\text{h}}/\mu_{\text{e}} = 1.47$) was achieved in the PTB7-Th:BTI2-30TPD blend, which explains the improvement of photocurrent in the all-PSCs.[22] The stepwise increasing and balanced charge mobilities for the neat and blend copolymer films provided further evidence of a preferential face-on orientation packing and reduced crystallinity in the BTI2-30TPD terpolymers, which has been discussed in the GIWAXS part.[23]

To demonstrate the generality of our method, a new terpolymer acceptor N2200-30TPD (30% TPD moiety) was synthesized via incorporating TPD as the third component into the classical N2200 polymer (Figure S8). We fabricated the all-PSCs based on PBT7-Th:N2200 and PBT7-Th:N2200-30TPD blends, respectively. The $J - V$ plots of the all-PSC devices based on two blends are shown in Figure S9. The all-PSC devices with N2200-30TPD as the electron acceptor showed improved J_{sc} and FF, resulting in an improved PCE of 4.03%, which is higher than that (PCE = 2.89%) of PBT7-Th:N2200 blend and the previous result (3.7%; Table S11).[7] This result indicates that our method is a general approach to optimize the active layer morphology and improve the device performance of all-PSCs.

Conclusions

In summary, a new series of BTI2-based n-type terpolymers BTI2-30BT, BTI2-30PhI, and BTI2-30TPD were successfully synthesized and characterized via random polymerization. Due to the incorporation of the BT, PhI and TPD units with different electron-accepting ability and solubility, distinct energy levels and crystallinity can be observed for the corresponding terpolymer structures. Furthermore, S, O, and N heteroatoms attached on the third components induced intramolecular noncovalent interactions, which can make a significant difference in the molecular planarity and packing structures. The elevated photovoltaic performance of the BTI2-30TPD-based devices was derived from the synergistic effects of the favorable face-on orientation and suitable crystallites, which demonstrated the significant advantages of TPD as a third component. TPD was also incorporated into the PTB7-Th: N2200 system, leading to an improved PCE. Consequently, these findings suggest that the introduction of an appropriate third electron-deficient building block into the polymer backbones can be an effective method for tuning the optoelectronic properties and crystallinity of the resulting terpolymer without sacrificing the electron mobilities, which can broaden the pool of polymer acceptors for highly efficient all-PSCs.

Experimental Section

Fabrication and Characterization of All-PSCs

The ITO glasses ($12\ \Omega\ \text{sq}^{-1}$) were cleaned according to a common procedure by sequential ultrasonic treatment in detergent, deionized water, acetone, and isopropanol for 15 minutes at each step. PEDOT:PSS (Clevios P VP A1 4083) was spin-coated onto UV–ozone (UVO) treated ITO substrates at 3000 rpm for 30 s and annealed at 150 °C for 15 min in air to form a ~40-nm film. Then the PEDOT:PSS-coated ITO substrates were transferred into a N_2-filled glove box for subsequent steps. The PTB7-Th:BTI2-FT and PTB7-Th:BTI2-30X solutions with various weight ratios were prepared with a total concentration of 16 mg mL^{-1} in chlorobenzene without any additives. The solutions were stirred overnight to achieve complete dissolution. The active layer with an optimal thickness of 120–150 nm was spin-coated onto the PEDOT:PSS layer. Then, 0.8 nm LiF and 110 nm Al were sequentially deposited atop the active layer via thermal evaporation under vacuum (*ca.* 1×10^{-5} Pa) to obtain an effective area of 0.045 cm^2 for the solar cells. Before evaluating the performance of the solar cells, all devices were thermally annealed at 80 °C for 5 min.

For device characterization, the current–voltage (*J–V*) characteristics of the devices were obtained under simulated AM 1.5G irradiation (100 mW/cm^2) using a Xe lamp-based SS-F5-3A solar simulator (Enli Technology, Inc.). A Xe lamp equipped with an AM 1.5G filter was used as the light source. The light intensity was controlled with an NREL-calibrated Si solar cell with a KG-5 filter. The EQE was collected using a QE-R3011 measurement system (Enli Technology, Inc.).

Funding Information

Acknowledgment

Supporting Information

Supporting information for this article is available online at http://doi.org/10.1055/s-0040-1713857.

References

(1) Heeger, A. J. *Adv. Mater.* **2014**, *26*, 10.

(2) (a) Yuan, J.; Zhang, Y.; Zhou, L.; Zhang, G.; Yip, H.-L.; Lau, T.-K.; Lu, X.; Zhu, C.; Peng, H.; Johnson, P. A. *Joule* **2019**, *3*, 1140. (b) Cai, F.; Zhu, C.; Yuan, J.; Li, Z.; Meng, L.; Liu, W.; Peng, H.; Jiang, L.; Li, Y.; Zou, Y. *Chem. Commun.* **2020**, *56*, 4340. (c) Li, S.; Li, C.-Z.; Shi, M.; Chen, H. *ACS Energy Lett.* **2020**, *5*, 1554. (d) Zhang, J.; Liu, W.; Xu, S.; Zhu, X. *Org. Mater.* **2019**, *1*, 30. (e) Liao, Q.; Kang, Q.; Yang, Y.; An, C.; Xu, B.; Hou, J. *Adv. Mater.* **2019**, *32*, 1906557. (f) Xu, X.; Feng, K.; Bi, Z.; Ma, W.; Zhang, G.; Peng, Q. *Adv. Mater.* **2019**, *31*, 1901872. (g) Ma, R.; Liu, T.; Luo, Z.; Guo, Q.; Xiao, Y.; Chen, Y.; Li, X.; Luo, S.; Lu, X.; Zhang, M. *Sci. China Chem.* **2020**, *63*, 325. (h) An, Q.; Ma, X.; Gao, J.; Zhang, F. *Sci. Bull.* **2019**, *64*, 504. (i) Cui, Y.; Yao, H.; Zhang, J.; Zhang, T.; Wang, Y.; Hong, L.; Xian, K.; Xu, B.; Zhang, S.; Peng, J. *Nat. Commun.* **2019**, *10*, 1. (j) Guo, Q.; Ma, R.; Hu, J.; Wang, Z.; Sun, H.; Dong, X.; Luo, Z.; Liu, T.; Guo, X.; Guo, X. *Adv. Funct. Mater.* **2020**, *30*, 2000383. (k) Yan, C.; Liu, T.; Chen, Y.; Ma, R.; Tang, H.; Li, G.; Li, T.; Xiao, Y.; Yang, T.; Lu, X. *Solar RRL* **2020**, *4*, 1900377. (l) Liu, T.; Gao, W.; Zhang, G.; Zhang, L.; Xin, J.; Ma, W.; Yang, C.; Yan, H.; Zhan, C.; Yao, J. *Solar RRL* **2019**, *3*,

▲

221

Organic Materials   B. Liu et al.   THIEME OPEN ACCESS   **Original Article**

1800376. (m) Liu, L.; Kan, Y.; Gao, K.; Wang, J.; Zhao, M.; Chen, H.; Zhao, C.; Jiu, T.; Jen, A. K. Y.; Li, Y. *Adv. Mater.* **2020**, *32*, 1907604. (n) Dong, Y.; Zou, Y.; Yuan, J.; Yang, H.; Wu, Y.; Cui, C.; Li, Y. *Adv. Mater.* **2019**, *31*, 1904601. (o) Li, K.; Wu, Y.; Li, X.; Fu, H.; Zhan, C. *Sci. China Chem.* **2020**, *63*, 490. (p) Sun, H.; Liu, T.; Yu, J.; Lau, T.-K.; Zhang, G.; Zhang, Y.; Su, M.; Tang, Y.; Ma, R.; Liu, B. *Energy Environ. Sci.* **2019**, *12*, 3328.

(3) (a) Zhang, K.; Xia, R.; Fan, B.; Liu, X.; Wang, Z.; Dong, S.; Yip, H. L.; Ying, L.; Huang, F.; Cao, Y. *Adv. Mater.* **2018**, *30*, 1803166. (b) Wang, G.; Melkonyan, F. S.; Facchetti, A.; Marks, T. J. *Angew. Chem. Int. Ed.* **2019**, *58*, 4129. (c) Hwang, Y.-J.; Earmme, T.; Courtright, B. A.; Eberle, F. N.; Jenekhe, S. A. *J. Am. Chem. Soc.* **2015**, *137*, 4424. (d) Lee, C.; Lee, S.; Kim, G.-U.; Lee, W.; Kim, B. J. *Chem. Rev.* **2019**, *119*, 8028. (e) Choi, J.; Kim, W.; Kim, S.; Kim, T.-S.; Kim, B. J. *Chem. Mater.* **2019**, *31*, 9057. (f) Feng, W.; Lin, Z.; Lin, C.; Wang, W.; Ling, Q. *ACS Appl. Mater. Interfaces* **2019**, *11*, 43441. (g) Chen, S.; An, Y.; Dutta, G. K.; Kim, Y.; Zhang, Z. G.; Li, Y.; Yang, C. *Adv. Funct. Mater.* **2017**, *27*, 1603564. (h) Fan, Q.; Su, W.; Chen, S.; Kim, W.; Chen, X.; Lee, B.; Liu, T.; Méndez-Romero, U. A.; Ma, R.; Yang, T. *Joule* **2020**, *4*, 658. (i) Yang, J.; Xiao, B.; Tang, A.; Li, J.; Wang, X.; Zhou, E. *Adv. Mater.* **2019**, *31*, 1804699. (j) Wang, W.; Wu, Q.; Sun, R.; Guo, J.; Wu, Y.; Shi, M.; Yang, W.; Li, H.; Min, J. *Joule* **2020**, *4*, 1070. (k) Fan, Q.; Ma, R.; Liu, T.; Su, W.; Peng, W.; Zhang, M.; Wang, Z.; Wen, X.; Cong, Z.; Luo, Z. *Solar RRL* **2020**, *4*, 2000142. (l) Wu, J.; Meng, Y.; Guo, X.; Zhu, L.; Liu, F.; Zhang, M. *J. Mater. Chem. A* **2019**, *7*, 16190. (m) Jia, T.; Zhang, J.; Zhong, W.; Liang, Y.; Zhang, K.; Dong, S.; Ying, L.; Liu, F.; Wang, X.; Huang, F. *Nano Energy* **2020**, *72*, 104718. (n) Zhou, K.; Wu, Y.; Liu, Y.; Zhou, X.; Zhang, L.; Ma, W. *ACS Energy Lett.* **2019**, *4*, 1057. (o) Sun, H.; Liu, B.; Koh, C. W.; Zhang, Y.; Chen, J.; Wang, Y.; Chen, P.; Tu, B.; Su, M.; Wang, H.; Guo, X. *Adv. Funct. Mater.* **2019**, *29*, 1903970. (p) Liu, X.; Li, X.; Li, Y.; Song, C.; Zhu, L.; Zhang, W.; Wang, H. Q.; Fang, J. *Adv. Mater.* **2016**, *28*, 7405.

(4) (a) Guo, Y.; Li, Y.; Awartani, O.; Han, H.; Zhao, J.; Ade, H.; Yan, H.; Zhao, D. *Adv. Mater.* **2017**, *29*, 1700309. (b) Kolhe, N. B.; Lee, H.; Kuzuhara, D.; Yoshimoto, N.; Koganezawa, T.; Jenekhe, S. A. *Chem. Mater.* **2018**, *30*, 6540. (c) Zhao, R.; Wang, N.; Yu, Y.; Liu, J. *Chem. Mater.* **2020**, *32*, 1308. (d) Liu, X.; Zhang, C.; Duan, C.; Li, M.; Hu, Z.; Wang, J.; Liu, F.; Li, N.; Brabec, C. J.; Janssen, R. A.; Bazan, G.C.; Huang, F.; Cao, Y. *J. Am. Chem. Soc.* **2018**, *140*, 8934. (e) Liu, S.; Chen, D.; Zhou, W.; Yu, Z.; Chen, L.; Liu, F.; Chen, Y. *Macromolecules* **2019**, *52*, 4359. (f) Zhao, C.; Wang, J.; Jiao, J.; Huang, L.; Tang, J. *J. Mater. Chem. C* **2020**, *8*, 28. (g) Meng, H.; Li, Y.; Pang, B.; Li, Y.; Xiang, Y.; Guo, L.; Li, X.; Zhan, C.; Huang, J. *ACS Appl. Mater. Interfaces* **2020**, *12*, 2733. (h) Duan, T.; Gao, J.; Babics, M.; Kan, Z.; Zhong, C.; Singh, R.; Yu, D.; Lee, J.; Xiao, Z.; Lu, S. *Solar RRL* **2020**, *4*, 1900472. (i) Lee, J.; Lee, S. M.; Chen, S.; Kumari, T.; Kang, S. H.; Cho, Y.; Yang, C. *Adv. Mater.* **2019**, *31*, 1804762. (j) Genene, Z.; Mammo, W.; Wang, E.; Andersson, M. R. *Adv. Mater.* **2019**, *31*, 1807275. (k) Jenekhe, S. A. *Adv. Mater.* **2016**, *28*, 124. (l) Wang, X.; Han, J.; Huang, D.; Wang, J.; Xie, Y.; Liu, Z.; Li, Y.; Yang, C.; Zhang, Y.; He, Z. *ACS Appl. Mater. Interfaces* **2020**, *12*, 20393. (m) Tang, A.; Xiao, B.; Wang, Y.; Gao, F.; Tajima, K.; Bin, H.; Zhang, Z. G.; Li, Y.; Wei, Z.; Zhou, E. *Adv. Funct. Mater.* **2018**, *28*, 1704507. (n) Xu, B.; Zheng, Z.; Zhao, K.; Hou, J. *Adv. Mater.* **2016**, *28*, 434. (o) Chen, K.; Ma, R.; Liu, T.; Luo, Z.; Xu, X.; Wang, Q.; Chen, Y.; Xiao, Y.; Lu, X.; Yan, H. *J. Mater. Chem. A* **2020**, *8*, 7083. (p) Liao, Q.; Sun, H.; Li, B.; Guo, X. *Sci. Bull.* **2019**, *64*, 1747. (q) Cai, Y.; Huo, L.; Sun, Y. *Adv. Mater.* **2017**, *29*, 1605437.

(5) (a) Yuan, J.; Xu, Y.; Shi, G.; Ling, X.; Ying, L.; Huang, F.; Lee, T. H.; Woo, H. Y.; Kim, J. Y.; Cao, Y. *J. Mater. Chem. A* **2018**, *6*, 10421.

(b) Yuan, J.; Zhang, C.; Chen, H.; Zhu, C.; Cheung, S. H.; Qiu, B.; Cai, F.; Wei, Q.; Liu, W.; Yin, H.; Zhang, R.; Zhang, J.; Liu, Y.; Zhang, H.; Liu, W.; Peng, H.; Yang, J.; Meng, L.; Gao, F.; So, S.; Li, Y.; Zou, Y. *Sci. China Chem.* **2020**. Doi: 10.1007/s11426-020-9747-9.

(6) Earmme, T.; Hwang, Y. J.; Subramaniyan, S.; Jenekhe, S. A. *Adv. Mater.* **2014**, *26*, 6080.

(7) Li, Z.; Xu, X.; Zhang, W.; Meng, X.; Ma, W.; Yartsev, A.; Inganaäs, O.; Andersson, M. R.; Janssen, R. A.; Wang, E. *J. Am. Chem. Soc.* **2016**, *138*, 10935.

(8) (a) Jung, J. W.; Jo, J. W.; Chueh, C. C.; Liu, F.; Jo, W. H.; Russell, T. P.; Jen, A. K. Y. *Adv. Mater.* **2015**, *27*, 3310. (b) Luo, Z.; Sun, R.; Zhong, C.; Liu, T.; Zhang, G.; Zou, Y.; Jiao, X.; Min, J.; Yang, C. *Sci. China Chem.* **2020**, *63*, 361. (c) Ma, R.; Chen, Y.; Liu, T.; Xiao, Y.; Luo, Z.; Zhang, M.; Luo, S.; Lu, X.; Zhang, G.; Li, Y. *J. Mater. Chem. C* **2020**, *8*, 909. (d) Li, S.; Wen, X.; Zhou, J.; Zheng, N.; Liu, L.; Xie, Z. *Org. Mater.* **2020**, *2*, 071.

(9) (a) Chen, D.; Yao, J.; Chen, L.; Yin, J.; Lv, R.; Huang, B.; Liu, S.; Zhang, Z. G.; Yang, C.; Chen, Y. *Angew. Chem. Int. Ed.* **2018**, *57*, 4580. (b) Dang, D.; Yu, D.; Wang, E. *Adv. Mater.* **2019**, *31*, 1807019. (c) Duan, C.; Li, Z.; Pang, S.; Zhu, Y. L.; Lin, B.; Colberts, F. J.; Leenaers, P. J.; Wang, E.; Sun, Z. Y.; Ma, W. *Solar RRL* **2018**, *2*, 1800247. (d) Kim, S. W.; Kim, H.; Lee, J.-W. Lee, C.; Lim, B.; Lee, J.; Lee, Y.; Kim, B. J. *Macromolecules* **2019**, *52*, 738.

(10) Saito, M.; Osaka, I.; Suda, Y.; Yoshida, H.; Takimiya, K. *Adv. Mater.* **2016**, *28*, 6921.

(11) (a) Wang, Y.; Yan, Z.; Uddin, M. A.; Zhou, X.; Yang, K.; Tang, Y.; Liu, B.; Shi, Y.; Sun, H.; Deng, A. *Solar RRL* **2019**, *3*, 1900107. (b) Wang, Y.; Guo, H.; Ling, S.; Arrechea-Marcos, I.; Wang, Y.; López Navarrete, J. T.; Ortiz, R. P.; Guo, X. *Angew. Chem. Int. Ed.* **2017**, *56*, 9924.

(12) Wang, Y.; Yan, Z.; Guo, H.; Uddin, M. A.; Ling, S.; Zhou, X.; Su, H.; Dai, J.; Woo, H. Y.; Guo, X. *Angew. Chem. Int. Ed.* **2017**, *56*, 15304.

(13) Zhang, Y.; Tang, L.; Sun, H.; Ling, S.; Yang, K.; Uddin, M. A.; Guo, H.; Tang, Y.; Wang, Y.; Feng, K. *Macromol. Rapid Commun.* **2019**, *40*, 1900394.

(14) Li, Y.; Tatum, W. K.; Onorato, J. W.; Zhang, Y.; Luscombe, C. K. *Macromolecules* **2018**, *51*, 6352.

(15) Rogers, J. T.; Schmidt, K.; Toney, M. F.; Kramer, E. J.; Bazan, G. C. *Adv. Mater.* **2011**, *23*, 2284.

(16) (a) Guo, X.; Zhou, N.; Lou, S. J.; Smith, J.; Tice, D. B.; Hennek, J. W.; Ortiz, R. P.; Navarrete, J. T. L.; Li, S.; Strzalka, J. *Nat. Photonics* **2013**, *7*, 825. (b) Liu, Y.; Zhang, Z.; Feng, S.; Li, M.; Wu, L.; Hou, R.; Xu, X.; Chen, X.; Bo, Z. *J. Am. Chem. Soc.* **2017**, *139*, 3356. (c) Zhou, D.; Liu, Z.; Zhu, D.; Yuan, X.; Bao, X.; Yang, R. *Org. Mater.* **2019**, *1*, 71. (d) Cai, G.; Zhu, J.; Xiao, Y.; Li, M.; Liu, K.; Wang, J.; Wang, W.; Lu, X.; Tang, Z.; Lian, J. *J. Mater. Chem. A* **2019**, *7*, 21432.

(17) (a) Li, G.; Wang, S.; Li, D.; Liu, T.; Yan, C.; Li, J.; Yang, W.; Luo, Z.; Ma, R.; Wang, X. *Solar RRL* **2020**, *4*, 1900453. (b) Miao, J.; Meng, B.; Liu, J.; Wang, L. *Org. Mater.* **2019**, *1*, 88.

(18) Kang, H.; Lee, W.; Oh, J.; Kim, T.; Lee, C.; Kim, B. J. *Acc. Chem. Res.* **2016**, *49*, 2424.

(19) (a) Zhang, Y.-D.; Shi, L.-T.; Chen, Y.-W. *Acta Polym. Sin.* **2019**, *50*, 13. (b) Yang, C.; Yuan, L.; Zhou, R.; Wang, Z.; Zhang, J.; Zhang, Y.; Lu, K.; Wei, Z. *Org. Mater.* **2020**, *2*, 026.

(20) (a) Sun, L.; Zeng, W.; Xie, C.; Hu, L.; Dong, X.; Qin, F.; Wang, W.; Liu, T.; Jiang, X.; Jiang, Y. *Adv. Mater.* **2020**, *32*, 1907840. (b) Luo, Z.; Liu, T.; Xiao, Y.; Yang, T.; Chen, Z.; Zhang, G.; Zhong, C.; Ma, R.; Chen, Y.; Zou, Y. *Nano Energy* **2019**, *66*, 104146. (c) Gao, W.; Liu,

THIEME
OPEN
ACCESS

T.; Sun, R.; Zhang, G.; Xiao, Y.; Ma, R.; Zhong, C.; Lu, X.; Min, J.; Yan, H. *Adv. Sci.* **2020**, 7, 1902657.

(21) Mihailetchi, V. D.; Wildeman, J.; Blom, P. W. *Phys. Rev. Lett.* **2005**, *94*, 126602.

(22) Bartesaghi, D.; Pérez Idel, C.; Kniepert, J.; Roland, S.; Turbiez, M.; Neher, D.; Koster, L. *Nat. Commun.* **2015**, *6*, 7083.

(23) Tumbleston, J. R.; Collins, B. A.; Yang, L.; Stuart, A. C.; Gann, E.; Ma, W.; You, W.; Ade, H. *Nat. Photonics* **2014**, *8*, 385.